analytical chemistry

pubs.acs.org/ac Article

Electrocatalysis of Copper Sulfide Nanoparticle-Engineered Covalent Organic Frameworks for Ratiometric Electrochemical Detection of Amyloid-β Oligomer

Yana Chen, Shuangling Wang, Jujie Ren, Haiyan Zhao, Min Cui, Na Li, Meng Li,* and Cong Zhang*

Cite This: *Anal. Chem.* 2022, 94, 11201−11208 Read Online

ACCESS | Metrics & More | Article Recommendations | Supporting Information

ABSTRACT: Amyloid-β oligomer (AβO) is widely regarded as a reliable biomarker for the early diagnosis of Alzheimer's disease (AD). In this study, a signal on−off ratiometric electrochemical immunosensor has been developed for ultrasensitive detection of AβO. To achieve the dual-signal ratiometric strategy, ultrasmall copper sulfide nanoparticle-engineered covalent organic framework hybrid nanocomposites (CuS@COFs) were utilized as excellent electrocatalysts toward hydroquinone (HQ) oxidation to produce detectable signals. Meanwhile, electroactive thionine (Thi) and Aβ antibody-modified gold nanoparticles (Thi-AuNPs-Ab bioconjugates) were designed as another electrochemical indicator. Based on these two signals, an ultrasensitive sandwich-like electrochemical immunosensor was established for AβO detection. The introduction of AβO resulted in a remarkable decline in the electrochemical signal of HQ but an increase in the signal of Thi. Under optimum conditions, the ratios between the double signals (I_{Thi}/I_{HQ}) showed a proportional linear relationship with the AβO concentration (1 pM−1 μM) with a low detection limit of 0.4 pM (S/N = 3), and the biosensor was able to determine the content of AβO in real cerebrospinal fluid samples with satisfactory results. The ratiometric strategy proposed in our study offers a sensitive and efficient approach for early diagnosis of AD, and this work will promote the further applications of engineered COFs in electrochemical sensors.

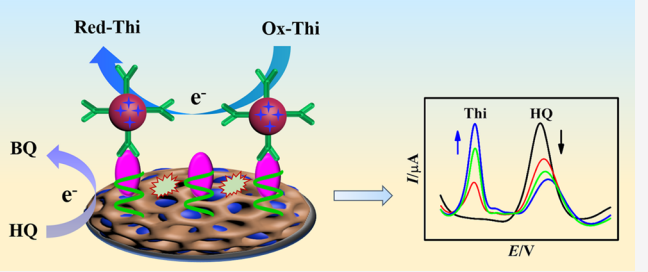

Alzheimer's disease (AD) clinically characterized by memory loss, selective neuronal death, and physical and behavioral dysfunction is the most prevalent type of dementia.[1,2] Recent studies reveal that amyloid-β peptide(Aβ) aggregation and accumulation are the key pathological factors involved in AD patients.[3,4] During the aggregation progression cascade, the formed intermediate Aβ oligomer (AβO) has been recognized as the most cytotoxic form. The level of AβO in cerebrospinal fluid (CSF) in AD patients is higher than that in normal groups.[5] AβO as an effective diagnostic marker can effectively predict the severity and progression at early or preclinical stages of AD.[6−8] Therefore, developing simple and fast assays for quantitative detection of AβO with high selectivity and sensitivity is vital for early diagnosis of AD.

Indeed, various methods have been employed to detect AβO including mass spectrometry,[9] transmission electron microscopy (TEM),[10] and polyacrylamide gel electrophoresis.[11] These methods are extremely time-consuming and low throughput. Considering the intrinsic features of AβO such as instability and easy transience to produce heterogeneous mixtures during the analysis process, fast detection is desirable for AβO sensors. To this aim, fluorescence assay,[12−14] enzyme-linked immunosorbent assay,[15] and surface plasmon resonance (SPR) biosensors[16,17] with the advantage of simplicity, low cost, and rapidity have attracted great attention in recent years. However, because of the great background signals, they are not suitable for studies in plasma. Detection of AβO in complex plasma with specific selectivity and high sensitivity is still a big challenge.

Electrochemical immunosensors that combine the advantages of electrochemistry and immunosensors provide a promising approach for both sensitive and selective analysis owing to their high compatibility and repeatability, simplified operation, as well as excellent controllability. To date, several studies utilizing electrochemical immune-sensing methods for AβO detection have been reported. For instance, Han's group employed ferrocene confined in a metal−organic framework as the electrochemical signal tag to develop an electrochemical immunoassay for highly sensitive detection of Aβ;[18] Lien et al. proposed a label-less impedimetric Aβ immunosensor based on the modified screen-printed electrode;[19] Qin et al. utilized an electrically conductive poly(pyrrole-2-carboxylic acid) linking agent and a PrP^C receptor to construct a label-free electro-

Received: April 12, 2022
Accepted: July 19, 2022
Published: August 3, 2022

https://doi.org/10.1021/acs.analchem.2c01602
Anal. Chem. 2022, 94, 11201−11208

chemical biosensor for selective detection of AβO.[20] Li et al. fabricated a signal-on biosensor based on the analyte-binding induced change of surface electron transfer for the quantitative determination of AβO.[21] Although promising, these methods are largely dependent on the transmitter and signal. Hence, external factors can easily interfere with the responsive signal, inducing the false-positive results.

The ratiometric electrochemical strategy utilizing the ratio of two signals from two different transmitters to provide a built-in correction to the interferences can significantly improve the reproducibility and precision of the electrochemical immunosensor. The key issue for constructing a ratiometric electrochemical immunosensor is to fabricate double spatial-resolved signals toward analytes in different response manners.

Covalent organic frameworks (COFs), as the newly emerged porous crystalline materials, are covalently assembled by organic building blocks. Because of the good thermal stability, high specific surface area, and unique ordered channel structures, COFs show a great potential for applications in a variety of research areas including gas adsorption, energy storage photovoltaic, and catalysis.[22,23] Moreover, the rich π-conjugation and multiple functional groups in frameworks enable COFs to be used as excellent scaffolds to establish immunosensors for the detection of biomarkers.[24−26] However, the poor electrical conductivity limited the application of COFs for fabricating electrochemical biosensors. Integrating COFs with metal nanoparticles (NPs) has been recognized as an effective method not only to enhance the electrochemical activity of COFs but also to offer a matrix to immobilize antibodies/aptamers,[27] which thus improves the sensing performance of electrochemical immunosensors. Combining the ratiometric strategy and COF-based nanomaterials may efficiently improve the sensitivity and selectivity of the biosensing platforms, giving rise to more accurate and reliable results.

In this work, we developed a novel signal on−off ratiometric electrochemical immunosensor for the ultrasensitive determination of AβO in the CSF sample based on the electrocatalytic activity of ultrasmall copper sulfide nanoparticle (CuS NP)-engineered COF hybrid nanocomposites (CuS@COFs) (Scheme 1). Briefly, the CuS@COFs were synthesized via a general encapsulation method. The introduction of CuS enabled the nanocomposites with electrocatalytic activity to catalyze the oxidation of hydroquinone (HQ) to *p*-benzoquinone (BQ), contributing to a large electrocatalytic signal. Besides, the fabricated CuS@COFs also served as substrates to immobilize the ssDNA aptamer. Taking advantage of the specific interaction between the targeted AβO and the ssDNA aptamer,[28] the aptamer-immobilized CuS@COFs (ssDNA-CuS@COFs)-modified electrode was employed for the capture of AβO. In the presence of AβO, AβO could bind to ssDNA-CuS@COFs, which hindered both the electron transfer and the exposure of the active sites, leading to a remarkable decline in the electrochemical signal of HQ. Subsequently, the electroactive thionine (Thi) and Aβ antibody-modified gold nanoparticles (AuNPs) (Thi-AuNPs-Ab bioconjugates) could bind to the targeted AβO to complete the sandwich immune interaction and produce another amplified electrochemical signal. As an excellent redox probe, Thi has been widely used in electrochemical biosensors.[29] Meanwhile, Thi could be self-assembled on AuNPs through Au−S binding.[29,30] AuNPs offer large surface areas for the conjugation of Thi and antibody, which can specifically

Scheme 1. Schematic Illustration for the Construction of CuS@COFs (A) and Thi-AuNPs-Ab Bioconjugates (B); (C) Schematic Diagram for the Fabrication of the Ratiometric Electrochemical Immunosensor

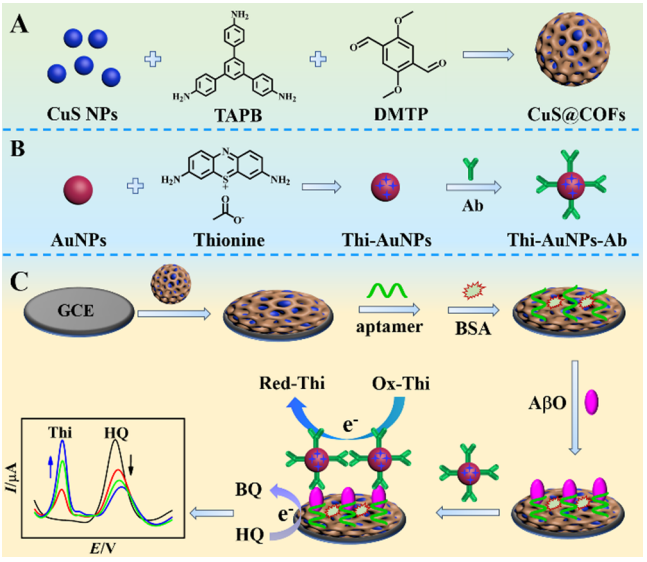

recognize the AβO, while the electroreduction of Thi can provide a measurable electrochemical signal, and the high loading of Thi on the AuNPs facilitates signal amplification, which results in enhanced sensitivity. On the basis of the two signal indicators, the dual-signal ratiometric immunosensor was successfully constructed for ultrasensitive determination of AβO both in solution and real CSF samples. This proposed biosensor holds a great potential for the development of reliable electrochemical devices for early diagnosis of complex diseases.

EXPERIMENTAL SECTION

Reagents and Materials. Amyloid-β (1−40) was purchased from Enzo (New York, USA). Anti-beta amyloid 1−40 antibody [EP1876Y] (ab76317) was supplied by Abcam. AβO and Aβ fibrils (AβF) were prepared according to previous work (see Supporting Information). Gold(III) chloride trihydrate and human serum albumin (HSA) were obtained from Sigma-Aldrich. 2,5-Dimethoxyterephthalaldehyde (DMTP), hydroquinone (HQ), 1,3,5-tris(4-aminophenyl) benzene (TAPB), thionin acetate (Thi), histidine (His), tryptophan (Trp), glycine (Gly), threonine (Thr), and bovine serum albumin (BSA) were bought from Aladdin Ltd. All aqueous solutions were prepared with doubly distilled deionized water (D.I. water). The AβO aptamer was purchased from Shanghai Sangon biotechnology, and its sequence was 5′-OH-$(CH_2)_6$-S-S-$(CH_2)_6$-GCCTGTGGTGTTGGGGCG-GGTGCG-3′.

Apparatus. The obtained nanocomposites were characterized by TEM (JEM-2100 microscope, Japan). Powder X-ray diffraction (XRD) profiles were collected using a SmartLab Focus diffractometer (Rigaku). X-ray photoelectron spectroscopy equipped with an Al Kα monochromated X-ray source (XPS, Thermo Scientific Escalab 250Xi, USA) was employed. Fourier transform infrared spectrum (FT-IR, TENSOR 37, Bruker, German) was collected. The UV−vis absorption spectra were recorded with a UV-5200 spectrophotometer (Shanghai Yuanxi). All the electrochemical experiments were

https://doi.org/10.1021/acs.analchem.2c01602
Anal. Chem. 2022, 94, 11201−11208

performed on a CHI660D electrochemical workstation. A conventional three-electrode system was employed with the modified glassy carbon electrode (GCE) as the working electrode, an Ag/AgCl electrode (saturated with KCl) as the reference electrode, and a platinum wire (1 mm diameter) as the counter electrode.

Synthesis of CuS@COFs. The citrate-coated CuS NPs were synthesized using a facile hydrothermal method. Briefly, copper(II) chloride (14 mg) and sodium citrate (20 mg) were dissolved in 100 mL of deionized (DI) water upon stirring at room temperature. After 5 min, sodium sulfide (7.8 mg) was added into the mixture, and then reacted at 25 °C overnight. After centrifugation at 15,000 rpm, the citrate-coated CuS NPs were obtained and washed with DI water three times. Finally, the obtained CuS NPs were dried at 60 °C in vacuum overnight.

Incorporating CuS NPs in COFs was performed using a general encapsulation method.[23,31] Briefly, 5.25 mg of TAPB and 2.5 mg of CuS NPs were dissolved in 1000 μL of *n*-butanol. Then, 25 μL of acetic acid (12 M) was added and stirred for 2 h at room temperature. Then, 1 mL of 1,4-ethylene oxide containing 4.35 mg of DMTP was added to the reaction system and stirred for another 2 h. Subsequently, 225 μL of acetic acid (12 M) was added, and the reaction was carried out at 70 °C for 24 h. The obtained CuS@COFs were washed with butanol, acetone, and water and dried under vacuum at room temperature overnight.

Synthesis of Thi-AuNPs-Ab Bioconjugates. First, citrate-stabilized AuNPs were synthesized according to a previous report with some modifications.[32] Briefly, 5 mL of $HAuCl_4$ (10 mM) was brought to a boil with vigorous stirring. Two minutes later, 5 mL of sodium citrate (38.8 mM) was added to the solution. After continuing to boil for 10 min, it was cooled to room temperature. Citrate-stabilized AuNPs were obtained by filtering. Subsequently, 0.22 mL of saturated Thi was added into 1.1 mL of AuNP solution and kept mixed for 24 h. Thi-AuNPs were washed with PBS and then dispersed in 0.2 mL of PBS. Finally, 5.71 μL of Aβ antibody (175 μg/mL) was added into Thi-AuNPs solution, and the solution was incubated for 24 h at room temperature. Then, BSA was added into the Thi-AuNPs-Ab biological coupling to seal the compound for 4 h. Finally, the Thi-AuNPs-Ab bioconjugates were obtained by centrifugation and washing, and then resuspended into 200 μL of 0.1 M PBS (pH 7.4).

Fabrication of the Immunosensor. First, the GCE was polished in turn with 0.3 and 0.05 μm α-alumina powder successively, followed by ultrasonic cleaning in water and ethanol. After that, 6 μL of CuS@COFs (1 mg/mL) was modified on the surface of GCE and dried at room temperature. Then, the CuS@COFs/GCE was immersed in 100 nM ssDNA aptamer solution at 4 °C for 12 h. After rinsing with water, the ssDNA-CuS@COFs/GCE was immersed in BSA solution (1 wt %) for 10 min to eliminate nonspecific binding sites. After rinsing, the BSA-ssDNA-CuS@COFs/GCE was incubated in 100 pM AβO solution at 25 °C for 60 min. Afterward, washing similarly, the AβO-BSA-ssDNA-CuS@COFs/GCE was immersed in Thi-AuNPs-Ab bioconjugate suspension at 25 °C for 80 min. Finally, the Thi-AuNPs-Ab-AβO-BSA-ssDNA-CuS@COFs/GCE was obtained. The whole preparation processes are illustrated in Scheme 1.

Effect of the pH Value of Working Buffer on the Electrochemical Signal. The electrochemical signal of the Thi-AuNPs-Ab-AβO-BSA-ssDNA-CuS@COFs/GCE was monitored using DPV by scanning the potential from −0.4 to 0.7 V in 0.1 M PBS containing 400 μM HQ with pH values ranging from 5.8 to 7.8.

Effect of Incubation Time of AβO and Thi-AuNPs-Ab Bioconjugates on the Electrochemical Signal. First, the BSA-ssDNA-CuS@COFs/GCE was incubated in 100 pM AβO solution at 25 °C with the incubation time ranging from 20 to 100 min. Then, the modified electrodes were rinsed with DI water, and the electrochemical signals were recorded using differential pulse voltammetry (DPV) by scanning the potential from −0.4 to 0.7 V in PBS (0.1 M, pH 7.0) containing 400 μM HQ. Next, the AβO-BSA-ssDNA-CuS@COFs/GCE was immersed in Thi-AuNPs-Ab bioconjugate suspension at 25 °C for different times (20−100 min). Then, the electrodes were rinsed, and the electrochemical signals were measured using DPV.

Effect of Incubation Temperatures of AβO and Thi-AuNPs-Ab Bioconjugates on the Electrochemical Signal. The BSA-ssDNA-CuS@COFs/GCE was incubated in 100 pM AβO solution under different temperatures (10, 15, 20, 25, 30, and 37 °C) with the incubation time of 60 min. For Thi-AuNPs-Ab bioconjugates, the AβO-BSA-ssDNA-CuS@COFs/GCE was immersed in Thi-AuNPs-Ab bioconjugate suspension under different temperatures (10, 15, 20, 25, 30, and 37 °C) with an incubation time of 80 min. Similarly, the electrodes were rinsed, and the electrochemical signals were measured using DPV.

Electrochemical Detection of AβO. To detect AβO, the BSA-ssDNA-CuS@COFs/GCE was incubated with different concentrations of AβO at 25 °C for 60 min. Afterward, the AβO-BSA-ssDNA-CuS@COFs/GCE was immersed in Thi-AuNPs-Ab bioconjugate suspension at 25 °C for 80 min. Finally, the modified electrode was washed for electrochemical measurements.

Electrochemical impedance spectroscopy (EIS) spectra were recorded in 0.1 M KCl solution containing 5.0 mM $[Fe(CN)_6]^{3-/4-}$ solution with the frequency ranging from 1×10^{-2} to 1×10^{5} Hz. Cyclic voltammetry (CV) measurements were performed in 0.1 M KCl solution containing 5.0 mM $[Fe(CN)_6]^{3-}$ with a scan rate of 100 mV s^{-1}. DPV measurements were carried out in PBS (0.1 M, pH 7.0) containing 400 μM HQ with scanning the potential from −0.4 to 0.7 V, the pulse amplitude of 50 mV, pulse width of 25 ms, and sampling width of 16.7 ms.

RESULTS AND DISCUSSION

Characterization of the Nanocomposites. TAPB and DMTP were employed as organic ligands to prepare CuS@COFs via the encapsulation method. The morphology of CuS NPs, COFs, and CuS@COFs were characterized by TEM. As shown in Figure 1A, the obtained COFs showed a spherical shape with an average diameter of around 400 nm, and CuS NPs were 13 nm in size with a spherical morphology (Figure 1B). Incorporating CuS NPs in the COFs did not change the morphology of COFs (Figure 1C). Furthermore, TEM elemental mappings of C, N, O, Cu, and S for CuS@COFs indicated that CuS NPs were homogeneously distributed and confined in the COFs (Figure 1D).

XRD was employed to investigate the structures of these nanocomposites. As indicated in Figure 2A, the diffraction 2θ peaks of pristine CuS NPs (curve a) were well-matched with the hexagonal phase of CuS NPs (JCPDS No. 06-0464). The diffraction peaks around 27.68°, 29.27°, 31.76°, 32.52°, 47.89°,

https://doi.org/10.1021/acs.analchem.2c01602
Anal. Chem. 2022, 94, 11201−11208

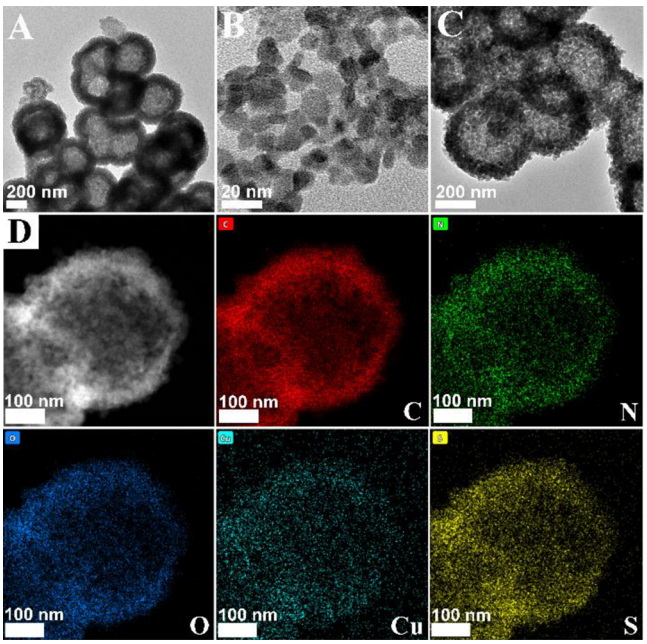

Figure 1. TEM images of COFs (A), CuS NPs (B), and CuS@COFs (C); EDS elemental mapping picture of CuS@COFs (D).

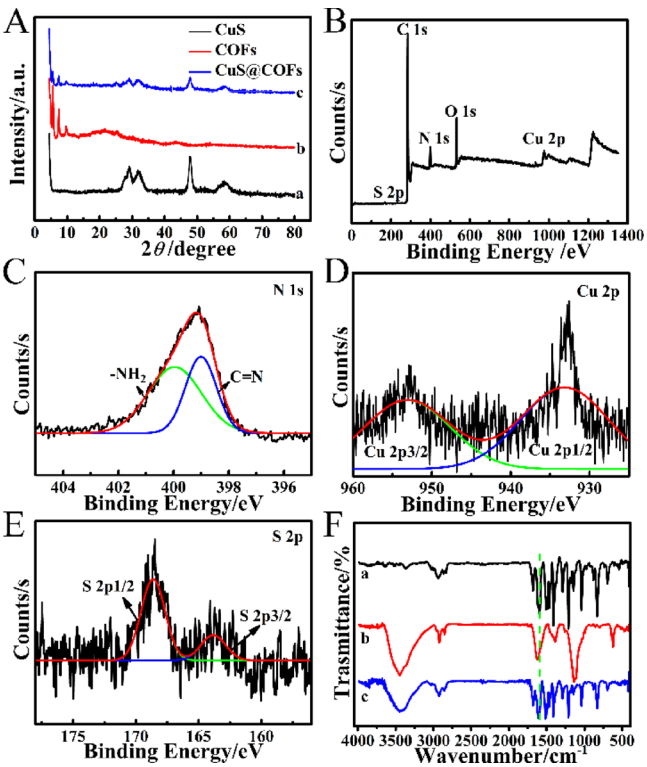

Figure 2. (A) XRD spectra of CuS (a), COFs (b), and CuS@COFs (c); (B) XPS full survey of the synthesized CuS@COFs; N 1s region (C), Cu 2p region (D), and S 2p region (E) in the XPS of the Cus@COFs composite; (F) FT-IR spectra of COFs (a), CuS (b), and CuS@COFs (c).

and 59.05° can be indexed to the (101), (102), (103), (006), (110), and (116) reflections of CuS NPs.[33] Besides, no obvious impurity peaks were observed, suggesting that CuS NPs have been successfully prepared. The strong diffraction intensity in curve b certified the fine crystallinity of COFs. The diffraction peaks appearing at 5.54°, 7.39°, 9.67°, and 25.36° were assigned to the lattice planes of (200), (210), (220), and (001),[34] respectively. For the CuS@COFs composites (curve c), the characteristic diffraction peaks of both CuS and COFs were presented, demonstrating that CuS@COF composites have been successfully synthesized.

Subsequently, the XPS analysis was applied to probe the chemical composition of CuS@COFs. The full wide-scan spectra revealed the existence of S, C, N, O, and Cu in CuS@COFs (Figure 2B). The N spectra exhibited two peaks at 401.4 and 399.8 eV (Figure 2C) corresponding to the residual $-NH_2$ groups and C═N in the COFs.[35] The peaks at 952.1 and 933.2 eV of Cu 2p spectra (Figure 2D) were ascribed to Cu 2p3/2 and Cu 2p1/2 doublets.[36] In the case of S 2p spectra (Figure 2E), two dominant peaks that appeared at 163.3 and 162.2 eV were assigned to S 2p1/2 and S 2p3/2 doublets, respectively.[36]

The successfully synthesized CuS@COFs were further confirmed by FT-IR spectroscopy (Figures S1 and 2F). In the spectra of COFs and CuS@COFs, the appearance at 1605 cm^{-1} belonged to the C═N band formed by the Schiff base reaction between TAPB and DMTP. A significant decrease in the intensity of −NH stretching bands of TAPB (3100−3500 cm^{-1}) and the C═O stretching bands of DMTP (1676 cm^{-1}) occurred (Figure S1). Meanwhile, the typical skeleton vibration bands of the benzene ring at 1600 to 1100 cm^{-1} were also observed. The peak at 618.3 cm^{-1} was due to the stretching vibrations of Cu−S.[37] All these results demonstrated that CuS NPs have been engineered in COFs.

The AuNPs were synthesized using citrate as the stabilizer and displayed an absorption peak at 520 nm (Figure S2) owing to the size-dependent surface plasmon resonance effect of the 15 nm AuNPs. The successful synthesis of the monodispersed AuNPs was also certified by the high-resolution TEM image (Figure S3). Incubation of AuNPs with Aβ antibody (for recognition of AβO) and Thi (for electrochemical signal amplification) generated the Thi-AuNPs-Ab bioconjugates. Also, an absorbance peak at 600 nm was observed in their UV−vis absorption spectrum (Figure S2), which was consistent with the reported results.[38]

Electrochemical Characterization of the Immunosensor Fabrication Process. EIS displayed the step-by-step decorating process of the immunosensor. The EIS results were fitted using ZSimpWin software with equivalent circuit models. As established in Figure 3A, the R_{ct} of bare GCE was measured to be 54.9 Ω. After CuS@COFs were modified, R_{ct} increased to 158.6 Ω mainly because of the steric hindrance of CuS@COFs. When the ssDNA aptamer was adsorbed on the surface of CuS@COFs, the R_{ct} increased to 260.9 Ω, which was attributed to the repulsion of the negatively charged $[Fe(CN)_6]^{3-/4-}$ from the surface of the GCE caused by the negatively charged phosphate backbone of the aptamer.[39] After blocking the ssDNA-CuS@COFs/GCE surface with BSA, the impedance was obvious increased, demonstrating that the protein hindered the electron transfer between the solution and the electrode surface. When the BSA-ssDNA-CuS@COFs/GCE was incubated with AβO, the Rct further increased. After Thi-AuNPs-Ab bioconjugates specifically bound to AβO, the resistance decreased mainly because the combination of AuNPs and Thi improved the conductivity and accelerated the electron transfer.

CV measurements were further employed to validate the EIS results. As displayed in Figure 3B, the bare GCE exhibited a

https://doi.org/10.1021/acs.analchem.2c01602
Anal. Chem. 2022, 94, 11201−11208

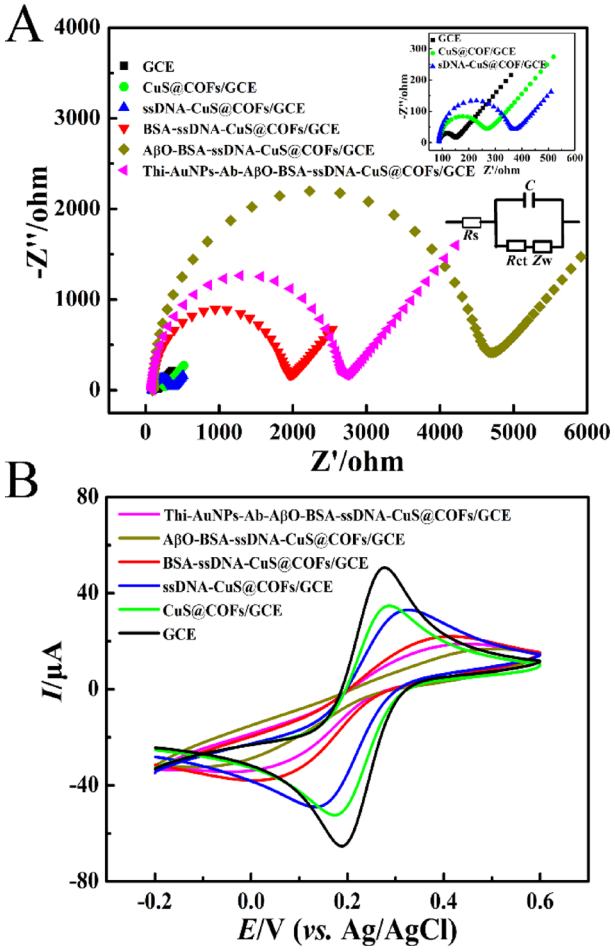

Figure 3. (A) EIS of bare GCE, CuS@COFs/GCE, ssDNA-CuS@COFs/GCE, BSA-ssDNA-CuS@COFs/GCE, AβO-BSA-ssDNA-CuS@COFs/GCE, and Thi-AuNPs-Ab-AβO-BSA-ssDNA-CuS@COFs/GCE in 0.1 M KCl solution containing 5.0 mM $[Fe(CN)_6]^{3-/4-}$ solution. The frequency range is from 1×10^{-2} to 1×10^5 Hz; (B) CV of bare GCE, CuS@COFs/GCE, ssDNA-CuS@COFs/GCE, BSA-ssDNA-CuS@COFs/GCE, AβO-BSA-ssDNA-CuS@COFs/GCE, and Thi-AuNPs-Ab-AβO-BSA-ssDNA-CuS@COFs/GCE in 0.1 M KCl solution containing 5.0 mM $[Fe(CN)_6]^{3-}$. Scan rate: 100 mV s^{-1}.

well-defined pair of redox peaks in a typical $[Fe(CN)_6]^{3-}$ solution. When CuS@COFs, ssDNA, BSA, AβO and Thi-AuNPs-Ab bioconjugates were modified onto the GCE surface layer by layer, the electron transfer was impeded due to the poor conductivity of each layer, so the redox peak currents decreased gradually in the following trend: bare GCE > CuS@COFs/GCE > ssDNA-CuS@COFs/GCE > BSA-ssDNA-CuS@COFs/GCE > Thi-AuNPs-Ab-AβO- BSA-ssDNA-CuS@COFs/GCE > AβO-BSA-ssDNA-CuS@COFs/GCE, which was consistent with the EIS results. These results demonstrated once again that each layer of materials was successfully fixed onto the GCE surface.

Feasibility of the Electrochemical Immunosensor. The electrochemical performance of the materials played a critical role in the feasibility of the fabricated ratiometric electrochemical immunosensor. To certify whether the nanocomposite displayed a good electrochemical response signal, the electrochemical performances of different modified electrodes were evaluated by DPV. As indicated in Figure S4, for CuS/GCE, a well-defined oxidation peak appeared, which attributed to the electro-catalytic oxidation of HQ. The COFs/GCE had no obvious oxidation peak. When CuS NPs were introduced to COFs, the peak current became larger, which demonstrated that CuS@COFs possessed an excellent electrocatalytic activity toward HQ. Hence, the HQ oxidation electrocatalyzed by CuS@COFs can act as an inner reference signal to construct a proportional sensor. By the stepwise modification of ssDNA and BSA, the peak currents slightly decreased because of the block effect of the attached biosubstances on the electron transfer. After capture of AβO by ssDNA aptamer, AβO located on the surface of CuS@COFs hindered both the electron transfer and the exposure of the active sites, leading to a remarkable decline in the current response of HQ. Upon further incubation with the saturated Thi-AuNPs-Ab bioconjugates, the current of HQ further decreased, accompanied by the synchronous emergence of a new redox peak of Thi at −0.18 V (Figure 4A), indicating the

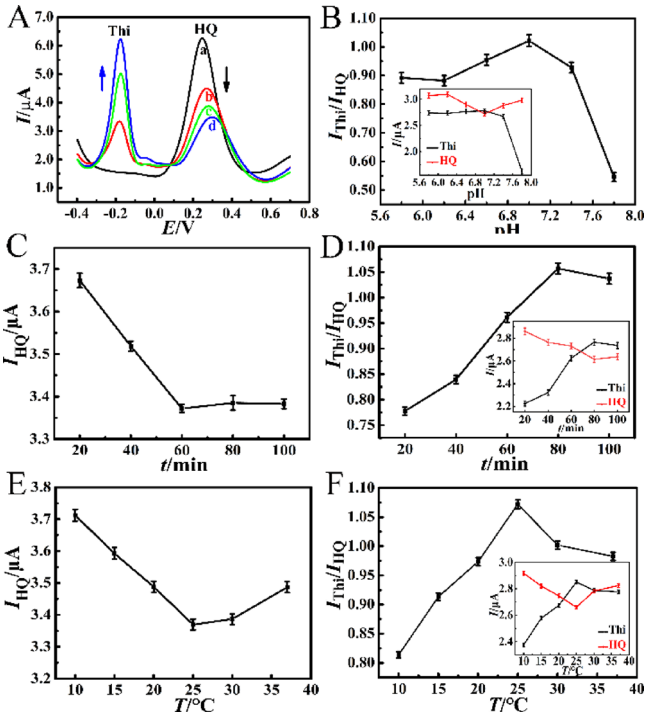

Figure 4. (A) Typical DPV curves of AβO-BSA-ssDNA-CuS@COFs/GCE (1 pM AβO) (a), Thi-AuNPs-Ab-AβO-BSA-ssDNA-CuS@COFs/GCE (1 pM AβO (b), 1 nM AβO (c), and 1 μM AβO (d)) in PBS (0.1 M, pH 7.0) containing 400 μM HQ; (B) influences of the pH (B), the incubation time of AβO (C) and Thi-AuNPs-Ab bioconjugates (D), and the incubation temperature of AβO (E) and Thi-AuNPs-Ab bioconjugates (F) on the response currents with 100 pM AβO in PBS (0.1 M, pH 7.0) containing 400 μM HQ.

efficient capture of the bioconjugates. As the signal amplification labels, AuNPs have been used widely in various biological detection schemes.[30,40,41] To verify the signal amplification capability of our proposed AβO detection method, four immunosensors were parallelly fabricated by coating Thi-AuNPs, Thi-Ab, AuNPs-Ab, and Thi-AuNPs-Ab films onto AβO-BSA-ssDNA-CuS@COFs/GCE, respectively, and their DPV responses were recorded and compared. As illustrated in Figure S5, a weak DPV current signal of Thi and an unchanged signal of HQ were observed for Thi-AuNPs films. The lack of Ab in the Thi-AuNPs films resulted in the

https://doi.org/10.1021/acs.analchem.2c01602
Anal. Chem. 2022, 94, 11201−11208

incapability of recognizing AβO-BSA-ssDNA-CuS@COFs and thus the failure to immobilize Thi-AuNPs on the electrode surface. The electrochemical signals of HQ obtained from Thi-Ab, AuNPs-Ab, and Thi-AuNPs-Ab film-modified AβO-BSA-ssDNA-CuS@COFs/GCE decreased significantly because the Ab captured AβO via specific interactions, which hindered both the electron transfer and the exposure of the active sites. In particular, for Thi-AuNPs-Ab bioconjugates, there was a significantly increased response current for the signal of Thi because the surface-captured AuNPs could load a large number of Thi molecules to enhance the current response,[30] indicating that AuNPs possessed remarkable signal amplification capability. Critically, as the concentration of AβO increased, the response signal of HQ decreased gradually while more signal probes of Thi-AuNPs-Ab bioconjugates were bound to the electrode surface and thus boosted the signal of Thi. Based on the signal generated by the CuS@COFs-mediated oxidation of HQ and the emergence of signals from the Thi-AuNPs-Ab bioconjugates, a facile ratiometric electrochemical immunosensor was fabricated to realize sensitive detection of AβO.

Optimization of Experimental Conditions. To achieve the best performance of the immunosensor, the experimental conditions such as the pH of the working buffer, incubation time, and temperature for AβO and Thi-AuNPs-Ab were optimized based on the peak current ratio of DPV signal responses (I_{Thi}/I_{HQ}).

The electrolyte pH had an important influence on the analytical response of the sensor. Figure 4B shows the effect of the electrolyte pH value on the DPV response of the signal of HQ and Thi in 0.1 M PBS containing 400 μM HQ with an incubation time of 60 min for AβO and ssDNA aptamer and 80 min for AβO and Thi-AuNPs-Ab bioconjugates at 25 °C. The electrochemical responses of HQ first decreased and then increased within the pH scope of 5.8−7.8. The result indicated that the optimal pH was pH 7.0. For the electrochemical signal of Thi, the response current achieved the maximum at pH 7.0 in the range of 5.8 to 7.0 and then decreased when further increasing the pH up to 7.8. Plainly, the I_{Thi}/I_{HQ} value showed a maximum at pH 7.0 (Figure 4B). Hence, pH 7.0 was chosen for the follow-up experiments.

The incubation times of AβO (Figure 4C) and Thi-AuNPs-Ab bioconjugates (Figure 4D) were also one of the main factors that can affect the electrochemical signal. Figure 4C shows that the response currents of HQ decreased with the incubation time ranging from 20 to 60 min and reached the steady state over 60 min, revealing that the combination of ssDNA aptamer and AβO reached saturation. The incubation time of Thi-AuNPs-Ab bioconjugates was also optimized based on the peak current ratio. As indicated in Figure 4D, the I_{Thi}/I_{HQ} value reached a maximum at 80 min, and then remained stable after 80 min, indicating the saturation of immobilized Thi-AuNPs-Ab bioconjugates after incubation for 80 min. Therefore, 60 and 80 min were chosen as the optimal incubation times for AβO and Thi-AuNPs-Ab bioconjugates, respectively.

In addition, the influence of incubation temperatures of AβO (Figure 4E) and Thi-AuNPs-Ab bioconjugates (Figure 4F) was also evaluated. When incubated AβO with BSA-ssDNA-CuS@COFs/GCE at 25 °C, the response current of HQ was minimum, indicating that 25 °C was the optimal incubation temperature for AβO and ssDNA aptamers. Similarly, as displayed in Figure 4F, the ratiometric signal of I_{Thi}/I_{HQ} reached its maximum value at 25 °C. Therefore, 25 °C was selected as the optimal incubation temperature for the binding of AβO and Thi-AuNPs-Ab bioconjugates.

Analytical Performance of the Electrochemical Immunosensor. The electrochemical signals were recorded by DPV under the optimal experimental conditions to examine the sensitivity of the prepared ratiometric electrochemical immunosensor. As shown in Figure 5A, with the increase in the AβO concentration, the HQ responses decreased while the Thi signals inversely increased, which endowed the sensor with a ratiometric mode for the assay of AβO. According to the ratio of the double signal (I_{Thi}/I_{HQ}), the prepared immunosensor could realize highly sensitive analysis of AβO. Figure 5B reveals that the value of I_{Thi}/I_{HQ} gradually increased with the increase in the AβO concentration. Also, the linear relationship of I_{Thi}/I_{HQ} to the logarithmic value of AβO concentration was plotted with a linear range from 1 pM to 1 μM and a correlation coefficient of 0.997. The regression equation was I_{Thi}/I_{HQ} (μA) = 0.298 log $C_{A\beta O}$ (nM) + 1.38, and the limit of detection (LOD) was calculated to be 0.4 pM (S/N = 3). Compared with other previous studies (Table 1), the fabricated electrochemical immunosensor exhibited much better sensing performance, which was attributed to the ratiometric strategy. In our sensing system, both of the response signals were dependent on AβO. In particular, the two signals appeared at different potentials (HQ at approximately +0.28 V and Thi at −0.18 V), which could not interfere with each other, and the two response intensities changed oppositely toward the target analytes, leading to a signal on−off mode.[42] This kind of signal on−off mode can not only correct the results by introducing the reference signal but also exclude the external interference. Moreover, COFs provided excellent scaffolds for aptamer

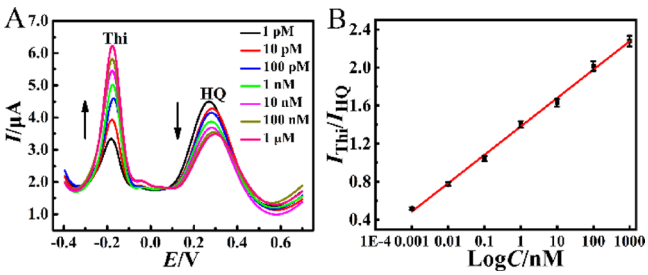

Figure 5. (A) DPV responses of the proposed ratiometric immunosensor in PBS (0.1 M, pH 7.0) containing 400 μM HQ after incubation with different concentrations of AβO; (B) dependence of the ratiometric signal of I_{Thi}/I_{HQ} on the logarithm AβO concentration in the range of 1 pM to 1 μM.

Table 1. Comparison of Different Methods for AβO Determination

methods	LOD	linear range	reference
SPR sensor	20.0 pM	0.02−1.0 nM	43
colorimetric assay	600 pM	10.5−313.5 nM	44
fluorescence strategy	28.4 pM	0.1−10,000 nM	14
fluorescence sensor	0.1 nM	0.1−40 nM	45
electrochemical assay	600 pM	5.0−5000 nM	46
electrochemical assay	30.0 pM	0.1−500 nM	39
electrochemical assay	3.5 pM	0.01−2.2 nM	47
electrochemical assay	8.0 pM	0.02−100 nM	48
electrochemical assay	26.0 pM	0.06−6.0 nM	49
electrochemical assay	0.4 pM	0.001−1000 nM	This work

https://doi.org/10.1021/acs.analchem.2c01602
Anal. Chem. 2022, 94, 11201−11208

attachment via $\pi-\pi$ stacking and hydrogen bonding interactions and AuNPs offered large surface areas for the conjugation of Thi and antibody, which were both beneficial for improving the sensitivity of the sensor and amplifying the signals. Therefore, the developed ratiometric electrochemical immunosensor could realize highly sensitive and accurate detection of AβO samples.

Specificity, Reproducibility, and Stability. To assess the specificity of the fabricated immunosensor, the effects of common interfering substances including Aβ monomers (AβM), AβF, HSA, BSA, Gly, Trp, and His on the sensing performance were investigated. Figures 6A and S6A show the

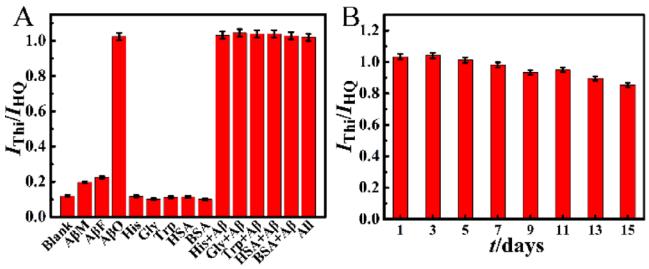

Figure 6. (A) Ratiometric signal of I_{Thi}/I_{HQ} responding to 100 pM AβO and some biological molecules; (B) stability of the immunosensor.

comparison of the electrochemical response toward AβM, AβF, and AβO. It was clear that the constructed immunosensor can only identify AβO but not AβM and AβF because of the high recognition ability of the aptamer to AβO. Obviously, other proteins and amino acids did not interfere with the detection of AβO (Figures 6A and S6B), indicating that the proposed electrochemical immunosensor displayed the satisfactory specificity for detecting AβO.

What's more, the reproducibility is another important parameter of sensors. The reproducibility of the sensor was investigated by conducting the repeated experiment with five independent electrodes. The relative standard deviation (RSD) obtained for the electrochemical signal was 2.5%, suggesting the excellent reproducibility of the sensor. Moreover, the long-term stability of the immunosensor was also evaluated by monitoring the electrochemical signals generated by 100 pM AβO every two days for two weeks. As shown in Figure 6B, after two weeks, the ratiometric signal of I_{Thi}/I_{HQ} of the immunosensor still remained 82.5% of their initial response. The results indicated that the designed immunosensor possessed good stability.

Application in CSF Samples. Inspired by the high selectivity and selectivity of the ratiometric electrochemical immunosensor toward AβO, we also examined whether the sensor can be used for the determination of AβO in real CSF samples, which was clinically meaningful for early diagnosis of AD. To assess the feasibility for real sample analysis, the detection of AβO was conducted using the standard addition method. Briefly, different concentrations of AβO were added to the CSF samples, and then, the concentration of AβO in CSF samples was measured using the designed immunosensor. As summarized in Table S1, the recovery values ranged from 95.2 to 105.7%, with the RSD below 4.1%, which demonstrated that the proposed sensing system can be applied for qualitatively detecting AβO in real CSF samples with good recovery and high precision.

CONCLUSIONS

In this work, a signal on−off ratiometric electrochemical immunosensor was successfully developed for ultrasensitive detection of AβO based on the signal changes of HQ oxidation catalyzed by CuS@COFs, and the signal arose from the Thi-AuNPs-Ab bioconjugates. Such a ratiometric electrochemical immunosensor exhibited a linear response to the concentration of AβO over the range of 1 pM to 1 μM with a detection limit of 0.4 pM. (S/N = 3). Critically, this immunosensor with excellent reproducibility, acceptable stability, high selectivity, and good accuracy has been successfully applied for detecting the AβO in real CSF samples. The dual-signal ratiometric electrochemical method can effectually eliminate the background signal drift to avoid the external interferences on the sensing performance, thus improving detection precision and clinical reliability. Our work shows a great potential for early diagnosis of AD and sheds light on developing a novel ratiometric electrochemical immunosensor for the analysis of other disease markers and will promote the further nanocomposite engineering of COF materials for bioapplications.

ASSOCIATED CONTENT

Supporting Information

The Supporting Information is available free of charge at https://pubs.acs.org/doi/10.1021/acs.analchem.2c01602.

FT-IR spectra of DMTP, TAPB, and COFs (Figure S1); UV−vis absorption spectra of AuNPs and Thi-AuNPs-Ab bioconjugates (Figure S2); TEM image of AuNPs (Figure S3); DPV response of different modified electrodes (Figure S4 and Figure S5); stability of the immunosensor (Figure S6); AβO and AβF preparation; and results of the detection of AβO in real CSF (Table S1) (PDF)

AUTHOR INFORMATION

Corresponding Authors

Meng Li − *Key Laboratory of Innovative Drug Development and Evaluation, College of Pharmaceutical Sciences, Hebei Medical University, Shijiazhuang 050017, China;* orcid.org/0000-0002-8348-6768; Email: limeng87@hotmail.com

Cong Zhang − *Hebei Provincial Key Laboratory of Photoelectric Control on Surface and Interface, College of Science, Hebei University of Science and Technology, Shijiazhuang 050018, China;* orcid.org/0000-0001-5023-5965; Email: zhangcong0672@163.com

Authors

Yana Chen − *Hebei Provincial Key Laboratory of Photoelectric Control on Surface and Interface, College of Science, Hebei University of Science and Technology, Shijiazhuang 050018, China*

Shuangling Wang − *Key Laboratory of Innovative Drug Development and Evaluation, College of Pharmaceutical Sciences, Hebei Medical University, Shijiazhuang 050017, China*

Jujie Ren − *Hebei Provincial Key Laboratory of Photoelectric Control on Surface and Interface, College of Science, Hebei University of Science and Technology, Shijiazhuang 050018, China;* orcid.org/0000-0002-2210-0294

Haiyan Zhao − *Hebei Provincial Key Laboratory of Photoelectric Control on Surface and Interface, College of*

Science, Hebei University of Science and Technology, Shijiazhuang 050018, China

Min Cui − *Hebei Provincial Key Laboratory of Photoelectric Control on Surface and Interface, College of Science, Hebei University of Science and Technology, Shijiazhuang 050018, China*

Na Li − *Hebei Provincial Key Laboratory of Photoelectric Control on Surface and Interface, College of Science, Hebei University of Science and Technology, Shijiazhuang 050018, China*

Complete contact information is available at: https://pubs.acs.org/10.1021/acs.analchem.2c01602

Author Contributions

Y.C. and S.W. contributed equally to this work. The manuscript was written through contributions of all authors. All authors have given approval to the final version of the manuscript.

Notes

The authors declare no competing financial interest.

■ ACKNOWLEDGMENTS

This work is funded by the Natural Science Foundation of Hebei Province (No. B2020208035, B2021208006, and H2021208004), the Youth Top-notch Talent Supporting Plan of Science and Technology Project of Hebei Education Department (No. BJ2021002), the Central Guidance on Local Science and Technology Development Fund of Hebei Province (226Z7715G and 226Z2601G), the Hundred Persons Plan of Hebei Province (E2018050012), the Youth Top-notch Talents Supporting Plan of Hebei Province (No. QNBJ19004), the National Natural Science Foundation of China (No. 21807024), and the Foundation of Hebei University of Science and Technology (No. 2021YWF22).

■ REFERENCES

(1) Liu, P. P.; Xie, Y.; Meng, X. Y.; Kang, J. S. *Sig. Transduct. Target. Ther.* **2019**, *4*, 29.
(2) Centeno, E. G. Z.; Cimarosti, H.; Bithell, A. *Mol. Neurodegener.* **2018**, *13*, 27.
(3) Viola, K. L.; Klein, W. L. *Acta Neuropathol.* **2015**, *129*, 183−206.
(4) Panza, F.; Lozupone, M.; Logroscino, G.; Imbimbo, B. P. *Nat. Rev. Neurol.* **2019**, *15*, 73−88.
(5) Mroczko, B.; Groblewska, M.; Litman-Zawadzka, A.; Kornhuber, J.; Lewczuk, P. *Int. J. Mol. Sci.* **2018**, *19*, 1884.
(6) Yin, Y.; Chen, G.; Gong, L.; Ge, K.; Pan, W.; Li, N.; Machuki, J. O.; Yu, Y.; Geng, D.; Dong, H.; Gao, F. *Anal. Chem.* **2020**, *92*, 9247−9256.
(7) Jamerlan, A.; An, S. S. A.; Hulme, J. *TrAc, Trends Anal. Chem.* **2020**, *129*, No. 115919.
(8) Li, C.; Lu, J.; Hu, X.; Feng, C.; Xiang, Y.; Karamanos, Y.; Li, G. *Part. Part. Syst. Charact.* **2018**, *35*, No. 1700384.
(9) Wang, J. S. H.; Whitehead, S. N.; Yeung, K. K. C. *J. Am. Soc. Mass. Spectrom.* **2018**, *29*, 786−795.
(10) Roberts, K. F.; Brue, C. R.; Preston, A.; Baxter, D.; Herzog, E.; Varelas, E.; Meade, T. J. *J. Inorg. Biochem.* **2020**, *213*, No. 111265.
(11) Pujol-Pina, R.; Vilaprinyó-Pascual, S.; Mazzucato, R.; Arcella, A.; Vilaseca, M.; Orozco, M.; Carulla, N. *Sci. Rep.* **2015**, *5*, 14809.
(12) Kulawik, A.; Heise, H.; Zafiu, C.; Willbold, D.; Bannach, O. *FEBS Lett.* **2018**, *592*, 516−534.
(13) Yu, H. J.; Zhao, W.; Xie, M.; Li, X.; Sun, M.; He, J.; Wang, L.; Yu, L. *Anal. Chem.* **2020**, *92*, 2953−2960.
(14) Fang, W.; Liu, L.; Zhang, L.; Liu, D.; Liu, Y.; Tang, H. W. *Anal. Chem.* **2021**, *93*, 12447−12455.
(15) Kim, J. A.; Kim, M.; Kang, S. M.; Lim, K. T.; Kim, T. S.; Kang, J. Y. *Biosens. Bioelectron.* **2015**, *67*, 724−732.
(16) Yi, X.; Feng, C.; Hu, S.; Li, H.; Wang, J. *Analyst* **2016**, *141*, 331−336.
(17) Zheng, Y.; Geng, X.; Yang, X.; Li, S.; Liu, Y.; Liu, X.; Wang, Q.; Wang, K.; Jia, R.; Xu, Y. *Anal. Chem.* **2020**, *92*, 2853−2858.
(18) Han, J.; Zhang, M.; Chen, G.; Zhang, Y.; Wei, Q.; Zhuo, Y.; Xie, G.; Yuan, R.; Chen, S. *J. Mater. Chem. B* **2017**, *5*, 8330−8336.
(19) Lien, T. T.; Takamura, Y.; Tamiya, E.; Mun'delanji, C. V. *Anal. Chim. Acta* **2015**, *892*, 69−76.
(20) Qin, J.; Jo, D. G.; Cho, M.; Lee, Y. *Biosens. Bioelectron.* **2018**, *113*, 82−87.
(21) Li, H.; Cao, Y.; Wu, X.; Ye, Z.; Li, G. *Talanta* **2012**, *93*, 358−363.
(22) Guan, X.; Chen, F.; Fang, Q.; Qiu, S. *Chem. Soc. Rev.* **2020**, *49*, 1357−1384.
(23) Shi, X.; Yao, Y.; Xu, Y.; Liu, K.; Zhu, G.; Chi, L.; Lu, G. *ACS Appl. Mater. Interfaces* **2017**, *9*, 7481−7488.
(24) Lu, J.; Wang, M.; Han, Y.; Deng, Y.; Zeng, Y.; Li, C.; Yang, J.; Li, G. *Anal. Chem.* **2022**, *94*, 5055−5061.
(25) Wang, M.; Lin, Y.; Lu, J.; Sun, Z.; Deng, Y.; Wang, L.; Yi, Y.; Li, J.; Yang, J.; Li, G. *Chem. Eng. J.* **2022**, *429*, No. 132332.
(26) Li, Y.; Liu, Z.; Lu, W.; Zhao, M.; Xiao, H.; Hu, T.; Ma, J.; Zheng, Z.; Jia, J.; Wu, H. *Analyst* **2021**, *146*, 979−988.
(27) Wang, M.; Lin, Y.; Wu, S.; Deng, Y.; Zhang, Y.; Yang, J.; Li, G. *Sens. Actuators, B* **2022**, *362*, No. 131813.
(28) Tsukakoshi, K.; Abe, K.; Sode, K.; Ikebukuro, K. *Anal. Chem.* **2012**, *84*, 5542−5547.
(29) Navaee, A.; Salimi, A. *J. Electroanal. Chem.* **2018**, *815*, 105−113.
(30) Yang, C.; Wang, Q.; Xiang, Y.; Yuan, R.; Chai, Y. *Sens. Actuators, B* **2014**, *197*, 149−154.
(31) Tan, J.; Namuangruk, S.; Kong, W.; Kungwan, N.; Guo, J.; Wang, C. *Angew. Chem., Int. Ed.* **2016**, *55*, 13979−13984.
(32) Xue, Q.; Niu, X.; Liu, P.; Wang, M.; Peng, Y.; Peng, H.; Li, X. *Sens. Actuators, B* **2021**, *334*, No. 129650.
(33) Palanisamy, S.; Velmurugan, S.; Yang, T. C. K. *Ultrason. Sonochem.* **2020**, *64*, No. 105043.
(34) Zhang, T.; Chen, Y.; Huang, W.; Wang, Y.; Hu, X. *Sens. Actuators, B* **2018**, *276*, 362−369.
(35) Zhang, C.; Cui, M.; Ren, J.; Xing, Y.; Li, N.; Zhao, H.; Liu, P.; Ji, X.; Li, M. *Chem. Eng. J.* **2020**, *401*, No. 126025.
(36) Liu, W.; Xu, H.; Liao, Y.; Quan, Z.; Li, S.; Zhao, S.; Qu, Z.; Yan, N. *Fuel* **2019**, *235*, 847−854.
(37) Dutta, S.; Ray, C.; Mallick, S.; Sarkar, S.; Sahoo, R.; Negishi, Y.; Pal, T. *J. Phys. Chem. C* **2015**, *119*, 23790−23800.
(38) Yu, Y.; Zhang, L.; Li, C.; Sun, X.; Tang, D.; Shi, G. *Angew. Chem.* **2014**, *126*, 13046−13049.
(39) Zhang, Y.; Figueroa-Miranda, G.; Lyu, Z.; Zafiu, C.; Willbold, D.; Offenhäusser, A.; Mayer, D. *Sens. Actuators, B* **2019**, *288*, 535−542.
(40) Wang, M.; Yin, H.; Zhou, Y.; Sui, C.; Wang, Y.; Meng, X.; Waterhouse, G. I. N.; Ai, S. *Biosens. Bioelectron.* **2019**, *128*, 137−143.
(41) Wang, M.; Pan, Y.; Wu, S.; Sun, Z.; Wang, L.; Yang, J.; Yin, Y.; Li, G. *Biosens. Bioelectron.* **2020**, *169*, No. 112638.
(42) Yang, J.; Hu, Y.; Li, Y. *Biosens. Bioelectron.* **2019**, *135*, 224−230.
(43) Xia, N.; Liu, L.; Harrington, M. G.; Wang, J.; Zhou, F. *Anal. Chem.* **2010**, *82*, 10151−10157.
(44) Zhou, Y.; Dong, H.; Liu, L.; Xu, M. *Small* **2015**, *11*, 2144−2149.
(45) Zhao, Y.; Li, X.; Yang, Y.; Si, S.; Deng, C.; Wu, H. *Biosens. Bioelectron.* **2020**, *149*, No. 111840.
(46) Huang, Y.; Zhang, B.; Yuan, L.; Liu, L. *Sens. Actuators, B* **2021**, *335*, No. 129697.
(47) Zhou, Y.; Lv, Y.; Dong, H.; Liu, L.; Mao, G.; Zhang, Y.; Xu, M. *Sens. Actuators, B* **2021**, *331*, No. 129429.
(48) Xia, N.; Wang, X.; Zhou, B.; Wu, Y.; Mao, W.; Liu, L. *ACS Appl. Mater. Interfaces* **2016**, *8*, 19303−19311.
(49) Duan, Y.; Chen, J.; Jin, Y.; Tu, Q.; Wang, S.; Xiang, J. *Anal. Chem.* **2021**, *93*, 3611−3617.